Dalton Transactions

Accepted Manuscript

This article can be cited before page numbers have been issued, to do this please use: D. Das, A. Ghosh, S. Ta, M. Ghosh, S. Karmakar, A. Banik, T. K. Dangar and S. K. Mukhopadhyay, *Dalton Trans.*, 2015, DOI: 10.1039/C5DT03431K.

This is an *Accepted Manuscript*, which has been through the Royal Society of Chemistry peer review process and has been accepted for publication.

Accepted Manuscripts are published online shortly after acceptance, before technical editing, formatting and proof reading. Using this free service, authors can make their results available to the community, in citable form, before we publish the edited article. We will replace this *Accepted Manuscript* with the edited and formatted *Advance Article* as soon as it is available.

You can find more information about *Accepted Manuscripts* in the Information for Authors.

Please note that technical editing may introduce minor changes to the text and/or graphics, which may alter content. The journal's standard Terms & Conditions and the Ethical guidelines still apply. In no event shall the Royal Society of Chemistry be held responsible for any errors or omissions in this *Accepted Manuscript* or any consequences arising from the use of any information it contains.

ROYAL SOCIETY OF CHEMISTRY

www.rsc.org/dalton

Dalton Transactions

Dynamic Article Links ▶
View Article Online
DOI: 10.1039/C5DT03431K

Cite this: DOI: 10.1039/c0xx00000x

www.rsc.org/xxxxxx

ARTICLE TYPE

Dual mode ratiometric recognition of zinc acetate: nano-molar detection with *in-vitro* tracking of endophytic bacteria in rice root tissue

Abhijit Ghosh[a] , Sabyasachi Ta[a] , Milan Ghosh[a], Subhajit Karmakar[b], Avishek Banik[c], Tushar Kanti Dangar[c], Subhra Kanti Mukherjee[d] and Debasis Das*[a]

Received (in XXX, XXX) Xth XXXXXXXXX 20XX, Accepted Xth XXXXXXXXX 20XX
DOI: 10.1039/b000000x

Single crystal X-ray structurally characterized several naphthalene based aldazine derivatives have been established as efficient colorimetric and fluorescence probes for selective ratiometric recognition of traces zinc acetate. Moreover, the probes are capable for *in-vitro* tracking of zinc acetate in endophytic bacteria within the rice root tissue. The probes are also useful to image zinc acetate in human breast cancer cells (MCF7) with normal as well as fluorescence microscopes. Density functional theoretical studies are in close agreement to the experimental findings.

Zinc[1] deficiency is treated by administration of different supplements like zinc gluconate (ZG), zinc gluconate-glycine (ZGG), zinc gluconate citrate (ZG-C) and zinc acetate (ZA) etc. Activity of zinc supplement depends on iZn (sum of all positive charged zinc species in solution) and the highest iZn value of ZA (100%) makes it most promising.[2]

Wilson's disease is treated with ZA that blocks the intestinal copper absorption from diet.[3] ZA lozenges are used to deal with common cold, cough, nasal discharge, and muscle ache.[4] It has mild antibacterial action and specific inhibitory effect against respiratory syncytial virus (RSV), the major cause of lower respiratory tract disease in children.[5, 6] Direct intra-tumoral ZA injection has positive impact to control prostate cancer growth.[7, 8]

Thus, sensitive and selective visual determination of traces ZA in human tumor and cancer cell lines after therapeutic treatment is very essential in medicinal chemistry. In literature, there are two available ZA selective probes,[9, 10] however none of them recognize ZA both colorimetric and ratiometric fluorescence method.

Addressing the limitations, herein, we report several probes for selective determination of traces ZA through ratiometric absorbance and fluorescence changes with improved detection limits and binding affinities at physiological conditions.

On the other hand, plant–microbe interactions that promote plant development and health has considerable research interest. Plants constitute vast and diverse niches for endophytic organisms. Among the microorganisms, endophytic bacteria occupy internal tissues of apparently healthy plant without substantive harm or benefit other than shelter, however provides beneficial effect.

Endophytic bacteria have agronomic interest as they may enhance plant growth in nonleguminous crops and improve their nutrition through nitrogen fixation, phosphate solubilisation or iron chelation. The interaction between plant and endophytic bacteria may have profound effect on plant health, growth, development, yield as well as soil quality as it reduces the consumption of chemicals, particularly for sustainable agriculture and environmental protection.[11-15] So, *in vitro* intra-cellular tracking of endophytic bacteria is one of the pioneering research interests of biologist to study their niche and interaction with the host. Detection of endophytic colonization and intracellular tracking of bacteria, transformation of green fluorescent protein (GFP) encoding plasmid is most popular for visualization. However, the method is very time consuming and expensive.[16, 17]

Our new probes successfully and efficiently track *in vitro* endophytic bacteria within six hours of infection in rice root tissue.

The probes are also useful to image ZA in human breast-cancer cells (MCF7) under fluorescence microscope.

Three probes, *viz.* A4, A5 and A6 are prepared by condensation of hydrazone derivative of 2-hydroxy-1-naphthaldehyde with different *p*- substituted benzaldehyde in methanol (Scheme 1). A model compound (A4a) has also been prepared using 1-naphthaldehyde instead of 2-hydroxy-1-naphthaldehyde (Scheme S1). The compounds have been characterized by ESI-TOF mass, ^{1}HNMR, ^{13}CNMR, FTIR spectra (Fig. S1–S19, ESI). Additionally, the structures of A4 and A6 have been confirmed by single crystal X-ray structure analysis (Fig. 1). Crystal packing and H-bonding network of A4 and A6 are presented in Fig. S20–S21 (ESI). Crystal parameters, refinement data, significant bond lengths and bond angles are summarized in Tables S1-S5 (ESI). Elemental analysis of the compounds are provided as evidence of their purities (ESI).

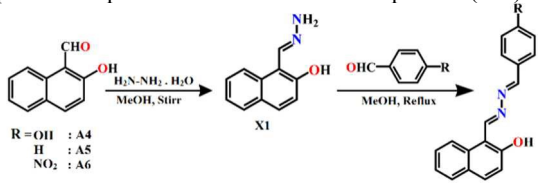

Scheme 1

Results and discussion

As the probes contain pH sensitive hydroxyl donor site, naturally their performance should be pH sensitive. Hence, the emission characteristics of A4 in presence and absence of ZA are examined at different pH. Fig. S22 (ESI) indicates that A4

View Article Online
DOI: 10.1039/C5DT03431K

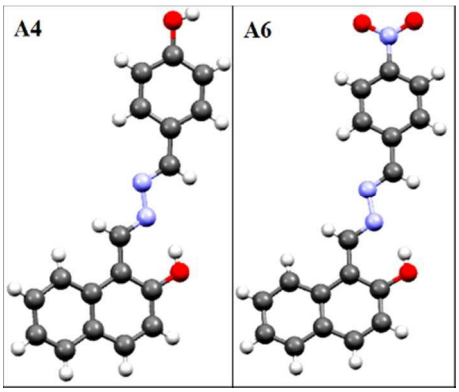

Fig. 1 Single crystal X-ray structures for A4 and A6

detects ZA over a wide range of pH from 6.0 to 12.0. Naturally, all experiments have been performed at pH 7.4, being closer to physiological pH. All spectral studies have been performed in 0.1 M HEPES buffered aqueous DMSO media (DMSO/ water, 9/1, v/v).

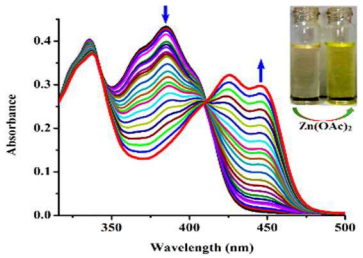

Fig. 2 Changes in the absorption spectra of A4 ((10 μM, DMSO–water (9: 1, v/v, 0.1 M HEPES buffer, pH 7.4) upon gradual addition of ZA (0-400 μM). Inset: naked eye colors of A4 before and after addition of ZA.

The binding and recognition events of the probes are studied using different spectroscopic methods. UV-Vis spectra of the solution of A4 (Fig. 2) reveals two absorption peaks at 335 nm (A5: 332 nm, A6: 333 nm; Fig. S23A) (π– π*) and 385 nm (A6: 381 nm, A6: 405 nm; Fig. S23B) (π– π*). Upon successive addition of ZA, the bands at 335 nm and especially at 385 nm gradually weakens with the appearance of a new red shifted band at 446 nm (A5: 444 nm, A6: 465 nm) and an isobestic point at 410 nm (A5: 401 nm, A6: 433 nm), indicating the formation of a new species (Fig. 3). The deprotonation of the naphthol group decreases the probability of π–π* transition energy decreases the probability of π– π* transition energy through improved delocalization[18] to account for the new red shifted band ~446 nm with the appearance of yellow- green (A5: yellow, A6: orange) coloration. The changes in the absorbance of the probes as a function of added ZA are presented in Fig. S24-S26 (ESI). The corresponding linear regions are useful for colorimetric determination of unknown ZA.

Fluorescence titrations of A4 (Fig. 4) and A5 (Fig. S27A, ESI) with varying concentration of ZA show that very weak emissions at 487 nm (for A4, λ_{ex}, 370 nm) and 495 nm (for A5, λ_{ex}, 430 nm) gradually increase with increasing ZA concentration. While for A6, the emission at 440 nm (λ_{ex}, 337 nm) gradually decreases (Fig. S27B, ESI) with the appearance of a new band at 520 nm. Emission intensities for A4, A5 and A6 increases with increasing ZA concentration (Fig. S28A, S29A and S30A). The linear region of those plots (Fig. S28B, S29B and S30B, ESI) are useful for determination of unknown ZA by fluorescence methods using A4, A5 or A6 respectively.

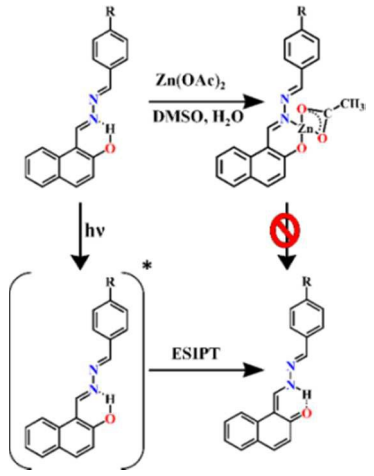

Fig. 3 Proposed $Zn(OAc)_2$ sensing mechanism

Fluorescence of the probes enhances when both Zn^{2+} and OAc^- ions are present together. Zn^{2+} salts of other counter anions or OAc^- salts of other metal ions do not show any fluorescence enhancement of A4 (Fig. 5 and 6). Common cations (Fig. S31, ESI) and anions (Fig. S32, ESI) do not interfere. The effect of other salts, including the acetate salts of different metal ions and zinc salts of different anions) on the absorption spectra of A4, A5 and A6 have also been studied. The results are included in ESI and indicate that the presence of both Zn^{2+} and OAc^- ions is must to observe the desired absorbance changes (Fig. S33, ESI).

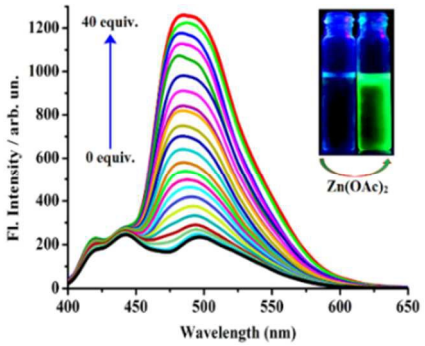

Fig. 4 Changes in the emission spectra of A4 (10 μM, same media as *supra*, pH 7.4, λ_{ex}, 370 nm, λ_{em}, 487 nm) upon gradual addition of ZA (0-400 μM). Inset: UV light exposed colors of A4 in absence and presence of ZA

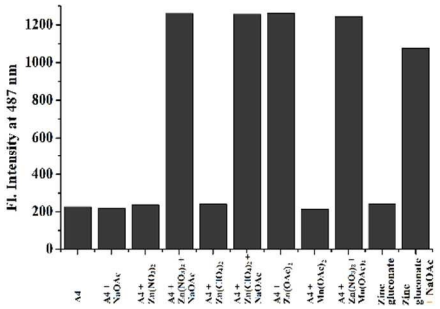

Fig. 5 Emission intensities of A4 (10 μM, DMSO–water (9: 1, v/v, 0.1 M HEPES buffer, pH 7.4, λ_{ex}, 370 nm; λ_{em}, 487 nm) in presence of different combinations of Zn^{2+} (400 μM) and/or OAc− (400 μM)

View Article Online
DOI: 10.1039/C5DT03431K

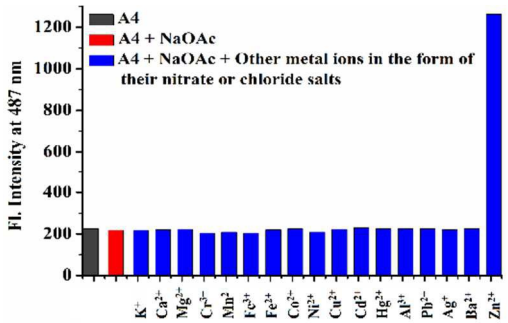

Fig. 6 Effect of different metal ions (400 μM) on the emission intensities of A4- OAc− (10 μM & 400 μM (DMSO– water, 9: 1, v/v, 0.1 M HEPES buffer, pH 7.4, λ_{ex}, 370 nm; λ_{em}, 487 nm) system

Very weak emission of the probes may be attributed to the excited state intra-molecular proton transfer (ESIPT) involving the naphthol proton and the imine nitrogen.[19] Upon interaction with ZA, the chelation-enhanced fluorescence (CHEF) starts and ESIPT stops (Fig. 3). It is found that increasing water content of the aqueous- DMSO media decreases the emission intensity of ZA adducts of A4, A5 and A6. Thus, the difference of emission intensities of the adducts with free probes decreases significantly, hindering the detection of ZA. Hence, we have used 10% aqueous-DMSO as optimum medium for spectral studies. This is attributed to the preferential coordination of water with Zn^{2+} over acetate at high water content. This is illustrated in Fig. S34 (ESI).

Introduction of electron withdrawing group at the *para* position of phenyl ring assists delocalization of the negative charge due to deprotonation of the naphthol proton. Consequently, the extent of π– π* transition energy decreases as reflected from the red shift in the emission as well as absorption maxima in A6 than that of A4 and A5. This fact has also been observed from the decrease of energy of both LUMOs (A4, – 1.7064 eV; A5, – 2.0634 eV and A6, – 3.0316 eV) and consequently the energy gap between frontier MOs of the probes (A4, 4.0466 eV; A5, 3.6180 eV and A6, 2.8534 eV) and their ZA complexes (A4, 3.3067 eV; A5, 3.3021 eV and A6, 2.3587 eV) upon changing 'R' from 'OH' to 'NO_2' through 'H' from A4 to A6 through A5 (Fig. 7-9). The decrease in energy of LUMO for A6 is so pronounced to give a very small gap between the frontier MOs resulting an intense emission at 440 nm for free A6. Thus, explaining the ratiometric emission changes of A6 in presence of $Zn(OAc)_2$. With the optimized structures of the complexes, electronic transition energies were calculated by the TDDFT method in the gas phase and in DMSO. For DMSO, the CPCM formalism was imposed which considers the solvent as a polarisable continuum and does not include discrete solvent molecules for solvation of the solute.[20] Calculated transition energies for the prominent absorption bands are shown in Table S6-S8 (ESI†). The calculated absorption peaks agree well with the experimentally observed peaks. Optimised structures for HOMO-1, HOMO-2 and HOMO-3 of A6 are presented in Fig. 10

For deeper insight on the nature of host–guest interaction, ^{1}H NMR titration of A4 with ZA has been performed in DMSO-d6 (Fig. 11). Interestingly, appearance of a very downfield proton (for naphthol –OH, δ 13.25 ppm) in A4 is attributed to the existence of intra-molecular H-bonding between imine nitrogen and naphthol –OH. The naphthol –OH is found to move downfield as one moves from free A4 (13.25 ppm) to A5 (13.40 ppm) to A6 (13.51 ppm). This is due to the stronger H-bonding provided by the more electron withdrawing group at the *para* position of phenyl ring. However, upon gradual addition of ZA to A4, the naphthol –OH weakens and eventually disappears at 1.0 equiv. ZA affirming coordination of the naphthol oxygen to ZA. Additionally, aldimine (–CH=N–) proton close to the naphthyl ring experiences an up-field shift from 9.72 ppm to 9.50 ppm. The –OH proton at the *para* position of the phenyl ring does not shift or disappear even after addition of 5.0 equiv. of ZA confirming its non-involvement to coordinate ZA. However, imine proton near to the phenyl ring and aromatic protons do not show any significant change, only a small up-field shift is attributed to "through bond delocalization" or "diamagnetic shielding" of the negative charge generated through deprotonation of naphthol –OH. No further change in the chemical shift values have been observed upon addition of ZA over 1.0 equiv. indicating a 1 : 1 stoichiometry between A4 and ZA which is further substantiated from Job's plot (Fig. S35, ESI) and mass spectra of their adducts with ZA (A4, Fig. S36; A5, Fig. S37, and A6, Fig. S38, ESI). The FTIR spectra of the ZA complexes of the receptors are shown in Fig. S39-S41, (ESI†). Inability of A4a to recognize ZA (Fig. S42, ESI) further establishes the requirement and involvement of naphthol oxygen donor for complex formation.

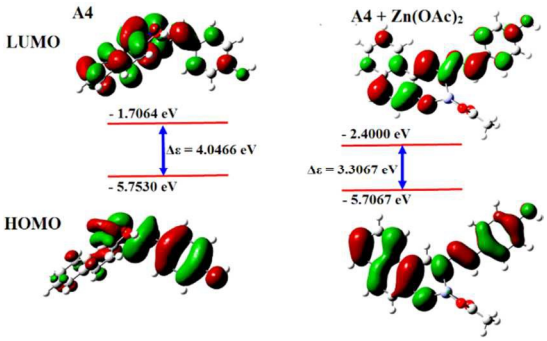

Fig. 7 Frontier molecular orbitals of **A4** and [**A4** + ZA] system

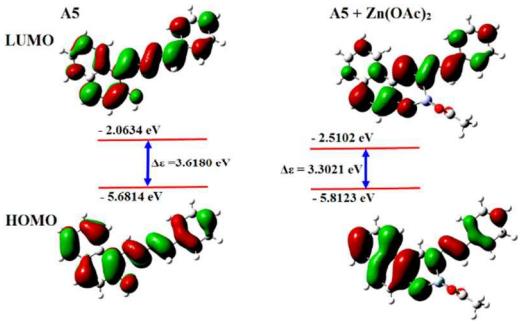

Fig. 8 Frontier molecular orbitals of **A5** and [**A5** + ZA] system

The binding constants of A4, A5 and A6 for ZA, evaluated from the respective fluorescence titrations are 3.9×10^5 M^-, 4.5×10^5 M^{-1} and 8.3×10^5 M^{-1} (Fig. S43, ESI) respectively, indicating a strong host-guest interaction. The increasing binding constants values from A4 to A6 are also in line with the aforesaid logic of extra stability gained by higher electron delocalization. The lowest detection limits of A4, A5 and A6 for ZA are 3.0×10^{-9} M, 8.1×10^{-9} M and 4.9×10^{-9} M (Fig. S44, ESI) respectively.

View Article Online
DOI: 10.1039/C5DT03431K

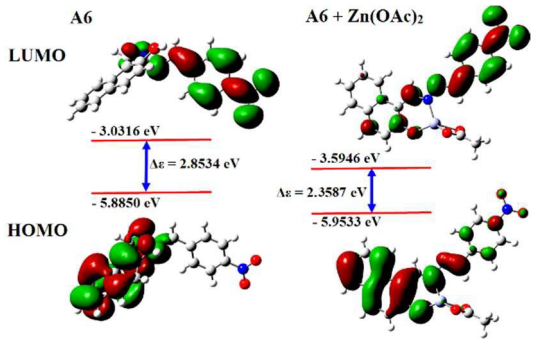

Fig. 9 Frontier molecular orbitals of **A6** and [**A6** + ZA] system

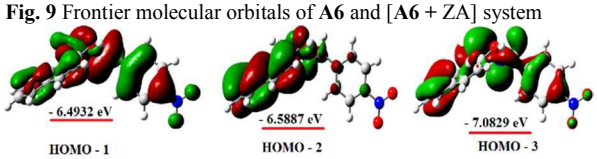

Fig. 10 HOMO-1, HOMO-2 and HOMO-3 of A6

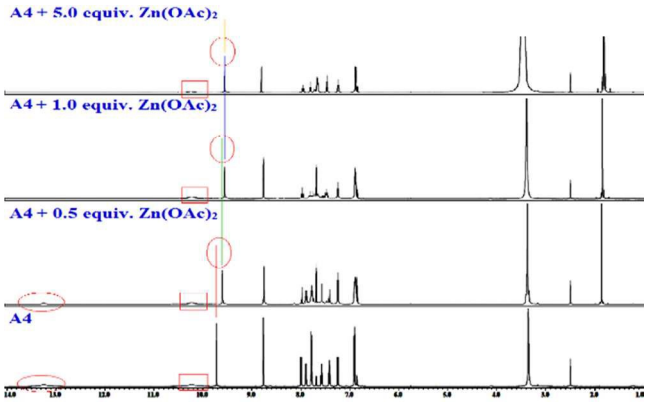

Fig. 11 ^{1}H NMR titration of A4 with ZA in DMSO-d6

Rice seedling imaging

After 6h incubation, ZA (100 µM) treated *A. chroococcum* cells have been infected within rice seedlings followed by A4 (10 µM) treatment. The lateral roots, especially at the zone of elongation and differentiation appear green when placed on the UV- transluminator (UV A) due to colonization of the bacterium (Fig. 12D). The phase contrast microscopy at 100_X magnification (UV-filter) of transverse section of those selected green emitting roots confirms the intra cellular localization of *A. chroococcum* inside root of *Oryza sativa var. Swarna* (Fig. 13C and D). No green emission has been observed from *A. chroococcum* used in control (Fig. 12A, B, C and Fig. 13A, B).

Human breast cancer (MCF7) cell imaging

Fig. 14 reveals that A4 is cell membrane permeable and detects intracellular ZA in human breast cancer cells (MCF7) under fluorescence microscope without any harm as cells remain alive even after several hours of exposure to 10 µM A4.

Experimental

Materials and methods

High-purity HEPES, hydrazine hydrate, 2-hydroxy-1-naphthaldehyde, 1-naphthaldehyde, benzaldehyde, 4-nitrobenzaldehyde and 4-hydroxybenzaldehyde are purchased from Sigma Aldrich (India). Solvents used are of spectroscopic grade. Other chemicals are of analytical reagent grade and have been used without further purification except when specified. Mili-Q Milipore 18.2 MΩ cm–1 water has been used throughout all the experiments. A Shimadzu Multi Spec 2450 spectrophotometer is used for recording UV-Vis spectra. FTIR spectra are recorded on a Shimadzu FTIR (model IR Prestige 21 CE) spectrophotometer. Mass spectra have been recorded using a QTOF 60 Micro YA 263 mass spectrometer in ES positive mode. ^{1}H NMR titration of A4 with ZA in DMSO-d_6 has been performed using a Bruker Avance 500 (500 MHz).^{13}C NMR spectrum of A4 and ^{1}H NMR spectra of A5 and A6 are recorded using a Bruker Avance 400 (400 MHz). While ^{13}C NMR spectrum of A5 and A6 and ^{1}H NMR spectra of X1 and X2 are recorded using a Bruker Avance 300 (300 MHz). Elemental analyses are performed on a Perkin Elmer 2400 CHN analyzer. The steady state emission and excitation spectra are recorded with a Hitachi F-4500 spectrofluorimeter. Systronics digital pH meter (model 335) is used for measurement of solution pH. Dilute HCl or NaOH (50 µM) are used for pH adjustment. The imaging system is composed of an inverted fluorescence microscope (Dewinter, Italy). Images are captured through an attached CCD camera equipped with BioWizard 4.2 software. The microscope is equipped with a 50 W mercury arc lamp. All spectra are recorded at room temperature.

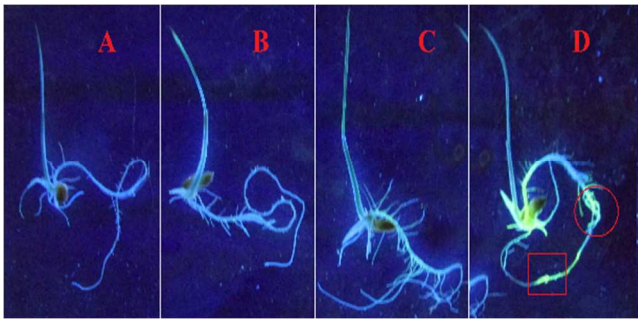

Fig. 12 Imaging of ZA in *A. A. chroococcum* cells infected within rice seedlings under UV- transluminator (UV A): (A) root, treated with suspension of *A. chroococcum* in sterile distilled water, (B) root, treated with ZA (100 µM) incubated *A. chroococcum*, (C) A4 (10 µM) treated root, incubated only with *A. chroococcum*, (D) root incubated with ZA (100 µM) and *A. chroococcum* followed by treatment with A4 (10 µM).

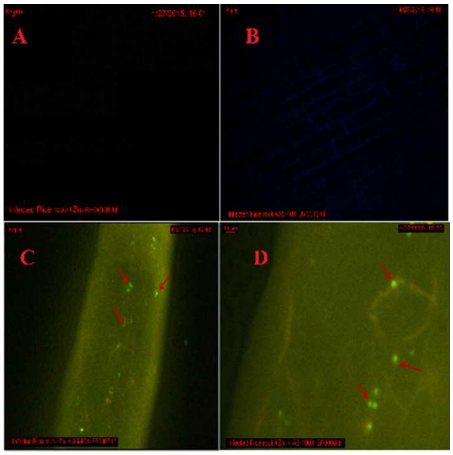

Fig. 13 Fluorescence microscope images of root (A) at 100x magnification, infected with ZA (100 µM) treated *A. chroococcum*; (B) at 40x magnification, infected with A4 (10 µM) treated *A. chroococcum*; (C) at 40x magnification, infected with and (D) at 100x magnification, infected with both ZA (100 µM) and A4 (10 µM) treated *A. chroococcum*

View Article Online
DOI: 10.1039/C5DT03431K

cells. Red arrow indicates localization of *A. chroococcum* cyst inside root of *Oryza sativa var. Swarna*.

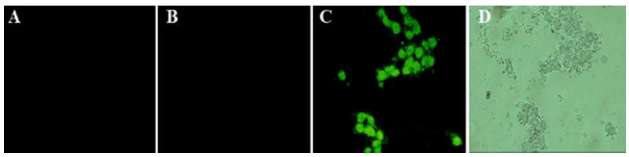

Fig. 14 Fluorescence microscope images of MCF7 cells: (A) and (B) are images of cells after 2 h incubation with ZA (100 μM) and A4 (10 μM) respectively, (C) cells after 2 h incubation with 100 μM ZA followed by addition of 10 μM A4 and (D) bright field image of the cells after incubation with 10 μM A4 for 2h followed by addition of 100 μM ZA.

General method of UV-Vis and fluorescence titration:

Path length of the cells used for absorption and emission studies is 1 cm. Stock solutions of A4, A5, A6 and ZA are prepared in DMSO/ water (9/1, v/v). Working solutions of A4, A5, A6 and ZA are prepared from their respective stock solutions. Fluorescence measurements are performed using 2.5 nm x 2.5 nm slit width.

Determination of binding constant:

The binding constant of A4, A5, A6 for ZA is determined using a modified Benesi–Hildebrand equation[21]:

$\frac{I_{max}-I_0}{I_x-I_0} = I + (\frac{1}{K})(\frac{1}{[C]^n})$; where I_{max}, I_0 and I_x are emission intensity values for A4, A5, A6 in the presence of ZA at saturation, in the absence of ZA and at any intermediate ZA concentrations, respectively. A plot of $\frac{I_{max}-I_0}{I_x-I_0}$ *vs.* $\frac{1}{[C]^n}$ (here n = 1.0) yields the binding constant values from the slopes.

Determination of detection limit:

From the fluorescence titration experiments, emission intensities at λem = 487 nm, 495 nm and 520 nm (for A4, A5 and A6 respectively) are normalized between the minimum and maximum values $\frac{I_x-I_0}{I_{max}-I_0}$; where I_{max}, I_0 and I_x are emission intensity values for A4, A5, A6 in the presence of ZA at saturation, in the absence of ZA and at any intermediate ZA concentrations in the low concentration regions, respectively. Linear regression curves are then fitted to the normalized data, and the points at which this line crosses the ordinate axes have been considered as the detection limits.[22] Detail calculations related to the determination of detection limits are listed in the ESI.

Synthesis of 1-hydrazonomethyl-naphthalen-2-ol (X1, Scheme 1):

10 mL (~ 200 mmol) hydrazine hydrate is taken in a 50 mL round bottom flask and placed over a magnetic stirrer. Another solution containing 2-hydroxy-1-naphthaldehyde (3.0 g, ~17.44 mmol) dissolved in minimum methanol is added drop wise with continuous stirring. After stirring for 6h, the solution is filtered off. The filtrate is then poured in 50 mL water whereby a precipitate appeared which is collected by filtration and dried in air. ESI-MS(+) m/z, Calculated for $C_{11}H_{10}N_2O$: 187.08; found: 187.02 $[M+H]^+$.

Synthesis of 1-[(4-hydroxy-benzylidene)-hydrazonomethyl]-naphthalen-2-ol (A4, Scheme 1):

A solution containing X1 (186 mg, ~1 mmol) and 4-hydroxybenzaldehyde (122 mg, ~1 mmol) in methanol is refluxed for 6h to get wine color solution which is kept in a test tube for slow evaporation. After several days X-ray quality needle shaped brown crystals appeared. Calculated yield: 70%. Anal. calcd (%): C, 74.47; H, 4.86 and N, 9.65; found: C, 74.43; H, 4.89 and N, 9.51. ^{1}H NMR [400 MHz, $CDCl_3$, TMS, J (Hz), δ (ppm)]: 13.25 (1H, s), 9.72 (1H, s), 8.76 (1H, s), 6.86 (2H, d, J = 8.25), 7.24 (1H, d, J = 7.8), 7.47 (2H, d, J = 8.20), 7.64 (1H, t, J = 8.0), 7.72 (1H, d, J = 7.80), 7.80 (1H, m, J = 8.0), 7.97 (1H, t, J = 7.8), 8.00 (1H, d, J = 8.0). ^{13}C NMR [400 MHz, $CDCl_3$, TMS, δ (ppm)]: 161.12, 149.31, 147.21, 134.24, 132.84, 129.22, 128.25, 127.84, 126.35, 124.95, 123.68, 120.18, 119.29, 114.57, 108.77. ESI-MS(+) (m/z), calculated for $C_{18}H_{14}N_2O_2$: 291.11; found: 291.2, $[M+H]^+$.

Synthesis of 1-[(benzylidene)-hydrazonomethyl]-naphthalen-2-ol (A5, Scheme 1):

A methanol solution of X1 (186 mg, ~1 mmol) is added to a methanol solution of benzaldehyde (106 mg, ~1 mmol). The resulting mixture is refluxed for 6h to obtain a yellow solution which on slow evaporation gives bright yellow solid. The product is recrystallized from DCM. Calculated yield: 87%. Anal. calcd (%): C, 78.81; H, 5.14 and N, 10.21; found: C, 78.75; H, 5.07 and N, 10.27. ^{1}H NMR [400 MHz, $CDCl_3$, TMS, J (Hz), δ (ppm)]: 13.40 (1H, s), 9.75 (1H, s), 8.65 (1H, s), 8.15 (1H, d, J = 8.4), 7.89 (3H, m, J = 6.4), 7.77 (1H, d, J = 7.6), 7.56 (1H, m, J = 6.0), 7.48 (3H, d, J = 6.0), 7.38 (1H, m, J = 6.8), 7.24 (1H, t, J = 5.2). ^{13}C NMR [300 MHz, $CDCl_3$, TMS, δ (ppm)]: 171.79, 161.58, 134.58, 133.71, 132.79, 131.50, 130.18, 129.37, 128.89, 127.85, 123.65, 120.07, 119.20, 108.23. ESI-MS(+), m/z: calculated for $C_{18}H_{14}N_2O$: 275.11. Found: 275.12, $[M+H]^+$; 297.08, $[M+Na]^+$.

Synthesis of 1-[(4-nitro-benzylidene)-hydrazonomethyl]-naphthalen-2-ol (A6, Scheme 1):

Condensation between X1 (186 mg, ~1 mmol) and 4-nitrobenzaldehyde (151 mg, ~1 mmol) as described above gives A4 as orange solid (Scheme 1) which is recrystallized from DCM to get X-ray quality needle shaped deep orange color crystals. Yield: 85%. Anal. calcd (%): C, 67.71; H, 4.10 and N, 13.16; found: C, 67.61; H, 3.96 and N, 13.24. ^{1}H NMR [400 MHz, $CDCl_3$, TMS, J (Hz), δ (ppm)]: 13.51 (1H, s), 9.76 (1H, s), 8.69 (1H, s), 8.19 (1H, d, J = 8.4), 7.99 (2H, t, J = 7.8), 7.93 (1H, d, J = 9.2), 7.84 (1H, d, J = 8.0), 7.79 (2H, d, J = 8.4), 7.63 (1H, m, J = 7.2), 7.45 (1H, t, J =7.6), 7.29 (1H, t, J = 2.0). ^{13}C NMR [300 MHz, $CDCl_3$, TMS, δ (ppm)]: 163.47, 161.76, 158.57, 139.56, 135.47, 132.77, 129.26, 129.14, 128.15, 124.07, 123.92, 119.94, 119.16. ESI-MS(+), m/z, Calculated for $C_{18}H_{13}N_3O_3$: 320.10; found: 320.19 $[M+H]^+$.

Synthesis of Naphthalen-1-ylmethylene-hydrazine (X2, Scheme S1):

X2 is prepared following the same procedure described above for X1 where naphthaldehyde (3.0 g, ~19.23 mmol) is used in place of 2-hydroxy-1-naphthaldehyde and reacted with10 mL (~

View Article Online
DOI: 10.1039/C5DT03431K

200 mmol) hydrazine hydrate. ESI-MS(+) m/z, Calculated for $C_{11}H_{10}N_2$: 171.08; found: 171.11 $[M+H]^+$.

Synthesis of 4-(naphthalen-1-ylmethylene-hydrazonomethyl)-phenol (A4a, Scheme S1):

A methanol solution containing X2 (170 mg, ~1 mmol) and 4-hydroxybenzaldehyde (122 mg, ~1 mmol) is refluxed for 6h. The resulting straw color solution is kept for slow evaporation to get a light yellow solid that is recrystallized from acetonitrile. The yield is 80%. Anal. calcd (%): C, 78.81; H, 5.14 and N, 10.21; found: C, 78.53; H, 5.23 and N, 9.98. ^{1}H NMR [400 MHz, $CDCl_3$, TMS, J (Hz), δ (ppm)]: 9.76 (1H, s), 9.12 (1H, s), 8.18 (1H, d, J = 7.6), 7.75 (4H, t, J = 8.4), 7.40 (1H, d, J = 6.8), 7.30 (1H, t, J = 8.0), 7.26 (2H, q, J = 3.2), 6.97 (3H, m, J = 4.4), 5.70 (1H, s). ESI-MS (+), m/z, calculated for $C_{18}H_{14}N_2O$: 275.11. found: 275.10 $[M+H]^+$.

Synthesis of ZA adducts of the probes:

To a magnetically stirred solution of A4 in acetonitrile, methanol solution of ZA (A4: ZA = 1: 1, mole ratio) is added drop-wise such that total solvent composition remains acetonitrile: methanol, 9:1 (v/v). After 10-15 min stirring, the solution is filtered and kept for slow evaporation while white solid appeared after several days.

The ZA complexes of A5 and A6 are prepared following the same procedure.

Rice seedling imaging

ZA (100 μM) is incubated with *Azotobacter chroococcum (16S rRNA gene NCBI acc. no. KP099933)* cells for 6h and infected within rice seedlings. Then, the system is treated with A4 (10 μM) and observed over UV- transluminator (UV A). Corresponding systems either without ZA or A4 are used as control.

Human breast cancer (MCF7) cell imaging

Human breast cancer cell line MCF7 are grown in DMEM (Sigma, St. Louis, USA) supplemented with 10% fetal bovine serum (Sigma, St. Louis, USA), 2 mM glutamine, 100 U mL^{-1} penicillin-streptomycin solution (Gibco, Invitrogen, USA) in presence of 5% CO_2 at 37°C. For *in vitro* imaging studies, the cells are seeded in 6 well culture plate with a seeding density of 10^5 cells per well. After reaching 60–70% confluence, the previous media is replaced with serum free media, supplemented ZA and A4 at a concentration of 100 and 10 μM, and incubated for 2h to facilitate their uptake by cells. The cells are then observed under an inverted microscope at different magnifications to examine any adverse effect on cellular morphology. A4 treated cells are then incubated with ZA alone for 15–30 min and observed under fluorescence microscope at different magnifications using blue filter. Images are captured through an attached CCD camera equipped with BioWizard 4.2 software. Control experiment is performed using medium devoid of ZA or A4.

Conclusions

For the first time, we report a dual mode ratiometric approach for colorimetric and fluorescence recognition of ZA using a single crystal X-ray structurally characterized naphthalene based aldazine probe. The CHEF assisted ESIPT inhibition is responsible for the sensing of ZA in aqueous solution with the best detection limit ever. *In-vitro* tracking of ZA in endophytic bacteria within the rice root tissue and intracellular imaging of ZA in human breast cancer cells (MCF7) has been performed with fluorescence microscope. Theoretical results are in full agreement to the experimental findings.

Acknowledgements

AG is grateful to BU for fellowship. ST and MG are grateful to UGC-DAE-CSR-Kolkata and State DST (Govt. of W.B.) for funding. We thank Dr A Banerjee, Department of Chemistry & Biochemistry, University of Texas at Austin, USA for routine cell imaging studies.

Notes and references

CCDC of A4 and A6 are 1018133 and 1415557.

[a]Department of Chemistry, The University of Burdwan, Burdwan, West Bengal, India. E-mail: ddas100in@yahoo.com; Fax: +91-342-2530452; Tel: +91-342-2533913

[b]University Science Instrumentation Center, The University of Burdwan, Burdwan, West Bengal, India.

[c]Microbiology Laboratory, Crop production division, ICAR- Central Rice Research Institute. Cuttack, Odisha, India.

[d]Department of Microbiology, The University of Burdwan, Burdwan, West Bengal, India.

Electronic Supplementary Information (ESI) available: [Schemes, tables, figures, and some spectra], See DOI: ######.

1 R. M. Roat-Malone. Bioinorganic Chemistry: A Short Course. Hoboken: John Wiley & Sons, 2002.

2 (a). G. A. Eby, *Bioscience Reports*, 2004, **24** (1), 23-39; (b). A. S. Prasad, F. W. J. Beck, B. Bao, D. Snell and J. T. Fitzgerald, *J. Infect. Dis.*, 2008, **197**, 795-802.

3 G. J. Brewer, Expert Opin. PharmOActher., 2001, **2** (9), 1473-1477.

4 A. S. Prasad, J. T. Fitzgerald, B. Bao, F. W. J. Beck and P. H. Chandrasekar, Ann. Intern Med., 2000, **133**, 249.

5 A. Osol, (ed.). Remington's Pharmaceutical Sciences. 16th ed. Easton, Pennsylvania: Mack Publishing Co., 1980., p. 718.

6 R..O. Suara, J. E. Jr. Crowe, *Antimicrob. Agents Chemother.*, 2004, **48** (3), 783-790.

7 M. R. Shah, C. L. Kriedt, N. H. Lents, M. K. Hoyer, N. Jamaluddin, C. Klein and J. Baldassare, *J. Exp. Clin. Canc. Res*., 2009, **28**, 84.

8 P. E. Spiess, Prostate Cancer - From Bench to Bedside, InTech, 2011

9 D. Karak, S. Das, S. Lohar, A. Banerjee, A. Sahana, I. Hauli, S. K. Mukhopadhyay, D. A. Safin, M. G. Babashkina, M. Bolte, Y. Garcia and D. Das, *Dalton Trans*., 2013, **42**, 6708

10 H. J. Zo, J. Y. Song, J. J. Lee, S. Velmathi and J. S. Park, *Talanta*, 2013, **112**, 80-84.

11 G. Welbaum, A.V. Sturz, Z. Dong and J. Nowak, *Crit. Rev. Plant. Sci*., 2004, **23**, 175–193.

12 D. Wilson, Oikos, 1995, 73(2), 274–276.

13 M. Rosenblueth and E. M. Romero, MPMI, 2006 (8), 827–837.

14 S. Compant, H. Kaplan, A. Sessitsch, J. Nowak, E. A. Barka and C. Clement, *Microbiol Ecol*., 2008, 63, 84–93.

15 G. Brader, S. Compant, B. Mitter, F. Trognitz and A. Sessitsch, *Curr. Opin. Biotechnol*., 2014, 27, 30–37.

16 R. Anand and C.P. Chanway, *Biol.Fert. of soils*, 2013, **49(1)**, 111-118.

17 A. Banik, S. K. Mukhopadhyay, A. Sahana, D. Das and T.K. Dangar, (2015). *Biol. Fert. Soils*, DOI: 10.1007/s00374-015-1064-6.

18 H. Qin, Y. He, C. Hu, Z. Chen and L. Hu, *Tetrahedron: Asymmetry*, 2007, **18**, 1769–1774.

19 M. Royzen, A. Durandin, V. G. Young, N. E. Geacintov and J. W. Canary, *J. Am. Chem. Soc*., 2006, **128**, 3854–3855.

20 (a) S. Miertus, E. Scrocco and J. Tomasi, *Chem. Phys*., 1981, **55**, 117; (b) M. Cossi, V. arone, R. Cammi and J. Tomasi, *Chem. Phys. Lett*., 1996, **255**, 327; (c) M. Cossi, V. Barone and M. A. J. Robb, *Chem. Phys*., 1999, **111**, 5295; (d) M. Cossi, G. Scalmani, N. Rega and V. J. Barone, *Chem. Phys*., 2002, **117**, 43.

21 H. A. Benesi and J. H. Hildebrand, *J. Am. Chem. Soc*., 1949, **71**, 2703-2707.

View Article Online
DOI: 10.1039/C5DT03431K

22 (a) M. Shortreed, R. Kopelman, M. Kuhn and B. Hoyland, Anal. Chem., 1996, **68**, 1414; (b) A. Caballero, R. Martinez, V. Lloveras, I. Ratera, J. V. Gancedo, K. Wurst, A. Tarraga, P. Molina and J. Veciana, J. Am. Chem. Soc., 2005, **127**, 15666; (c) S. Das, A. Sahana, A. Banerjee, S. Lohar, D. A. Safin, M. G. Babashkina, M. Bolte, Y. Garcia, I. Hauli, S. K. Mukhopadhyay and Debasis Das, Dalton Trans., 2013, **42**, 4757; (d) A. Ghosh, A. Sengupta, A. Chattopadhyay and D. Das, Chem. Commun., 2015, **51**, 11455.

View Article Online
DOI: 10.1039/C5DT03431K

Graphical abstracts

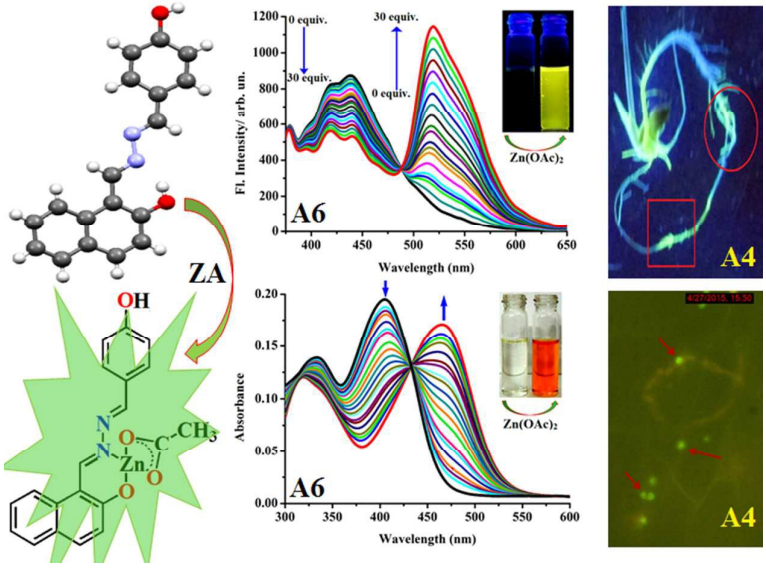

Structurally characterized naphthalene based aldazine derivatives efficiently detect traces zinc acetate (ZA) in a ratiometric manner both by fluorescence and naked eye. *In-vitro* tracking of ZA in endophytic bacteria within the rice root tissue and intracellular imaging of ZA in human breast cancer cells (MCF7) have been performed with fluorescence microscope. Density functional theoretical studies fully support the experimental findings.